Modeling of multienergy polygeneration hybrid system for the control strategies of the smart microgrid at the ENEA Research Center in Portici

Salvatore Fabozzi[1*], Francesco Pannone[2], Raffaele Iossa[2], Amedeo Buonanno[1], Giovanna Adinolfi[1], Giuseppe Langella[2], Alfredo Gimelli[2], Maria Valenti[1]

[1]*ENEA, Italian National Agency for New Technologies, Energy and Sustainable Economic Development* Portici, Naples, Italy
[2]*Industrial Engineering Department, University of Naples Federico II,* Naples, Italy

**Corresponding author:salvatore.fabozzi@enea.it*

***Abstract*— In response to the pressing need for sustainable energy solutions amidst escalating climate change challenges, the integration of polygenerative hybrid systems within smart microgrids has emerged as a promising avenue. This article delves into the modeling intricacies of such systems, focusing on the ENEA Research Center in Portici, Italy. Employing advanced simulation techniques and control strategies, the study elucidates the interplay between thermal and electrical components within smart microgrids. By leveraging TRNSYS software, the research assesses the efficacy of various control strategies in optimizing energy utilization and mitigating environmental impacts. Through comprehensive analysis and evaluation of multiple control strategies, the study not only contributes to the field of sustainable energy but also offers practical insights for policymakers and energy planners. Results underscore the significance of control strategies, with certain approaches demonstrating primary energy savings and CO_2 emissions avoidance.**

Keywords*— *smart microgrid, polygeneration, smart systems control strategies.

I. INTRODUCTION

In the face of rapidly evolving climate patterns and the escalating need for sustainable energy solutions, the integration of polygenerative hybrid systems within smart microgrids emerges as a promising avenue for addressing energy challenges[1]. As climate change intensifies, the imperative to adopt resilient and adaptive energy infrastructure becomes increasingly urgent. Microgrids, particularly those integrating both thermal and electrical components, represent a pivotal innovation in this pursuit, offering enhanced efficiency, reliability, and environmental sustainability.

Located at the forefront of the design and construction of the smart microgrid endeavor is the ENEA Research Center in Portici, Italy. Situated within a context of dynamic climate shifts and mounting energy demands, the center serves as a crucible for pioneering advancements in energy technology and infrastructure. Against this backdrop, the modeling and analysis of polygenerative hybrid systems within smart microgrids assume paramount significance, offering insights into effective control strategies for optimizing energy utilization and mitigating environmental impacts [2][3].

A. Beyond the state of art

The advancement in the state of the art of smart energy grids is evident through the comparison with existing projects. The Smart Polygeneration Microgrid (SPM) [4] at the Savona Campus in Italy [5] and the FortZED Projects demonstrator in Fort Collins, USA [6], bear similarities to the proposed SEM (Smart Energy Microgrid) but exhibit notable differences. The SEM stands out for its experimental focus on testing various operational logics of the integrated energy system. Unlike other projects that primarily target specific functionalities like active load management or energy optimization, the SEM's central control operates at both hierarchical levels at the same time, demonstrating adaptability and flexibility in managing interconnected sub-networks. This design reflects the real-world scenario where pre-existing subnets require integration into a multi-energy system. Moreover, the SEM accommodates significant critical loads, such as the CRESCO6 HPC data center, distinguished by its substantial computing power ranking among the world's top supercomputers. Such critical loads pose unique challenges and necessitate robust management strategies. These differences underscore the novelty of the SEM proposal, which not only addresses technical complexities but also emphasizes adaptability and integration within existing infrastructure, setting a new benchmark in smart energy grid design and implementation. Through a comprehensive examination of polygenerative hybrid systems, control strategies, and the simulation forecast [8][9][10][11] this research not only contributes to the burgeoning field of sustainable energy but also offers practical insights for policymakers, energy planners, and researchers grappling with the imperative of transitioning towards a low-carbon future.

II. METHOD AND TOOL

The hybrid PV-Wind-CHP system was modeled and dynamically simulated using the TRNSYS software [12] . This software tool is extensively utilized in both commercial and scientific domains for conducting sophisticated multipurpose analyses of hybrid, and innovative energy systems, enabling simulations close to reality [13], [14]. These models are either experimentally validated or intrinsically validated based on manufacturer data, ensuring the reliability of the simulation results [15]. The model simulated represents a portion of the SEM in Portici. It includes dual PV installations with a peak power of 175 kW, a 6 kW wind turbine, an energy storage system with a nominal capacity of 445 Ah, which can be charged by the 60 kW PV array, a 50 kW_{el} nominal cogenerator, a boiler, ENEA's electrical and thermal loads and the connection to the national electrical grid. A scheme of the energetic interaction between the energy conversion and storage systems of the SEM with the user's demand is represented Fig. 1.

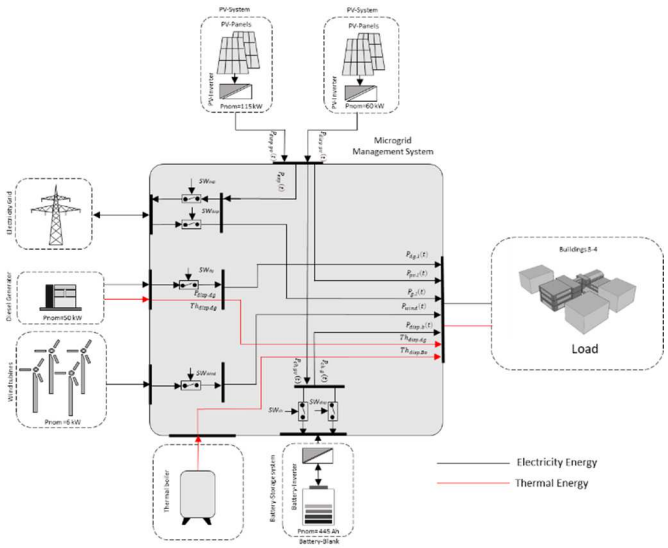

Fig. 1 Scheme of the interaction between the energy conversion and storage systems Smart microgrid

Here *below in section A, B, C, D*, we provide only a brief overview of the primary system component models, as detailed descriptions are available in the software reference [16].

A. Building Model

In this section, it has been described the ENEA's "Smart Multienergy Microgrid," focusing on the evaluation of energy loads and, consequently, the characterization of the user. This evaluation aims at designing and implementing an energy model, a smart multienergy microgrid, in line with the European Mission Innovation project [17]. For the dynamic load analysis, it has been considered the energy requirements of buildings 3 and 4, as depicted in Fig. 2.

Building three spans four floors, housing offices, two large laboratories including a heavily energy-consuming CRESCO (Computational Research Center for Complex Systems) located underground, an atrium with elevators and staircases, and a cafeteria on the second floor. On the other hand, building 4, facing the sea, comprises offices entirely, along with small adjacent laboratories. The two buildings were divided into 14 thermal zones (described in TABLE I) based on their uses and three shadow zones (Shading Group), representing nearby structures affecting the exposure of the studied buildings. These shadow zones, depicted as purple cubes within the project, include the CNR building and buildings 1 and 2 of ENEA.

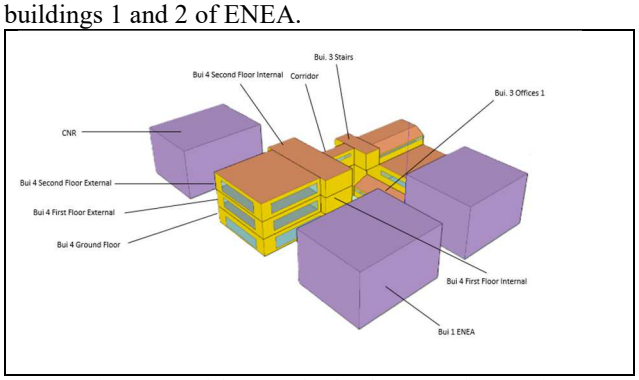

Fig. 2 3D model In Google SketchUp - North-West view

For simulating the building's thermal behavior, Type 56 was employed, while the geometric structure of the building was implemented using the SketchUp TRNSYS3d plug-in (thermal model). This tool facilitated the faithful reproduction of the buildings' geometry, position, orientation, solar radiation exposure, and wind influence, varying across hours, days, weeks, and months throughout the entire solar year, while considering the influence of surrounding buildings. This design approach enabled the hourly evaluation of temperature fluctuations across different thermal zones throughout the year, particularly considering the mutual influences among these zones and their adjacencies.

TABLE I Features of the identified thermal zones.

Thermal Zones	***Occupancy***	***Computers***	***Lights***	***Area (m^2)***
Bui. 3 Offices 1	5	12	27	95
Bui. 3 Offices 2	8	12	18	126
Bui.3 Offices 3	10	16	28	176
Bui.3 Laboratory 1	3	32	342	
Bui. 3 Cafeteria	30	--	36	216
Bui. 3 Atrium Stairs	2	--	10	80
Bui 3 Stairs 2	1	--	6	60
CRESCO Laboratory	3	1875*	10	342
Bui 4 First Floor External	10	30	80	504
Bui 4 First Floor Internal	6	12	48	216
Bui. 4 Second Floor External	10	30	80	504
Bui. 4 Second Floor Internal	6	12	48	216
Bui. 4 Ground Floor	16	32	128	500
Corridor	--	--	10	32

[a] *The number is referred to the equivalent PC

B. PV panels

The TRNSYS component chosen to model the electrical performance of a PV array is the "Type 94"[18]. For crystalline modules, whether monocrystalline or polycrystalline, the component utilizes a four-parameter equivalent circuit model as depicted in Fig. *3*.

The equivalent circuit (Fig. 3) consists of a direct current source, a diode, and a resistor, where:

- I_L is the PV current dependent on temperature and irradiance.
- I_D is the diode current flowing internally through the p-n junction. The diode represents the p-n junction of the cell.
- R_S is the resistance accounting for internal electrical dissipations of the individual cells constituting the module, such as electrical contacts.

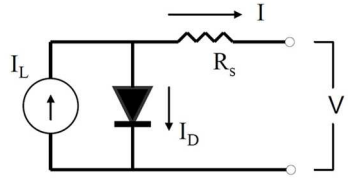

Fig. 3 Equivalent Circuit of a PV Cell

Other models, those with five parameters, in addition to the series resistance, also take into account a parallel resistance to the diode, the so-called "Shunt Resistance," which considers that part of the electrical energy generated is dissipated due to manufacturing and production defects of the cell, meaning that the cell does not exhibit ideal behavior In a study [19], it has been shown that even if considered low, its effect on power is negligible; therefore, in this study, it will be neglected. In the four-parameter model, the "Shunt Resistance" is assumed to be infinite.

C. Battery

In this work we assume using a lead-acid battery, the TRNSYS component used to model the electrical storage system is the "Type 47." The model equations describing the battery are those devised by Shepherd.
During the discharging phase (I<0), the battery voltage can be evaluated as follows:

$$V = e_{qd} - g_d \cdot H + I \cdot r_{qd} \cdot \left(1 + \frac{m_d \cdot H}{\frac{Q_d}{Q_m} - H}\right) \qquad (1)$$

Conversely, during the charging phase (I>0), the voltage can be expressed as follows:

$$V = e_{qd} - g_c \cdot H + I \cdot r_{qc} \cdot \left(1 + \frac{m_c \cdot H}{\frac{Q_c}{Q_m} - H}\right) \qquad (2)$$

Where:
V is the battery voltage; I is the charging/discharging current of the battery; e_{qc}, e_{qd} are the open circuit voltages at full charge and full discharge respectively; H is the complement of the battery charge percentage: H = (1 - F); g_c and g_d are coefficients of H during charging and discharging respectively; r_{qc}, r_{qd} are the internal resistances at full charge during charging and discharging respectively; Q_m is the nominal cell capacity [Ah]; Q_c and Q_d are capacity parameters during charging and discharging respectively; m_c, $m_d$are cell parameters.
The calculations are performed on a single cell, but the power input or output refers to the entire battery consisting of n cells in series or parallel.

D. Wind tubines

The TRNSYS component used to model the mini wind turbine system is the "Type 90." The model has the following assumptions in order to write mass, momentum, and energy balances:
- Constant and incompressible flow
- No mass flow through the boundary of the flow tube
The equation utilized to expresso the power (P_D) can be writer as follow:

$$P_D = \frac{1}{2}\rho_{AIR} \cdot A_{ROT} \cdot V_{wind}^3 \qquad (3)$$

E. CHP

The TRNSYS component used to simulate the performance of the internal combustion engine in cogeneration mode is the "Type 120". In addition to this component, a calculator was also utilized to determine the total thermal power that can be cogenerated. This is derived from the recovery of thermal energy from exhaust gases and jacket cooling, the electrical efficiency of the cogenerator, and the volumetric flow rate of fuel required to meet the load. The cogenerable thermal power is evaluated as follows:

$$Q_{COG} = 0.0079 \cdot P_{EL}^2 + 0.884 \cdot P_{EL} + 18.94 \qquad (4)$$

The electrical efficiency of the cogenerator is evaluated using the following equation:

$$\eta_{EL} = -0.00002 \cdot P_{EL}^2 + 0.299 \cdot P_{EL} + 1.64 \qquad (5)$$

Where P_{EL} in The electric power generated.
Finally, the volumetric flow rate of fuel is expressed as follows:

$$V_{CH_4} = -0.0008 \cdot P_{EL}^2 + 0.299\, P_{EL} + 1.64 \qquad (6)$$

The equations have been obtained taking into account the parameters provided by [20]

F. Energy Model

The equation that allows to derive the fossil primary power consumed by the separate system is as follows:

$$P_{P,SEP} = \left[\frac{\dot{Q}_{TH,heat}}{SCOP} \cdot \frac{1}{\eta_{EL,}}\right] + \left[\frac{P_{EL,CHP}}{\eta_{EL,}}\right] + \left[\frac{\dot{Q}_{TH,DHW}}{\eta_{Boiler}}\right]$$

This equation is expressed in terms of powers as the Primary Energy Saving (PES) is calculated on an hourly basis. In the second term of the right-hand side, the first term represents the useful power requested by the user, while the second term represents all the electrical power produced by the CHP.
The equation that allows us to derive the fossil primary power consumed by the cogeneration system is as follows:

$$P_{P,COG} = [\dot{m}c \cdot H_i]$$

Simply put, the only consumption of hourly primary power is the one provided to the cogenerator.
Finally, the PES is given by:

$$PES_{CHP} = \frac{P_{P,SEP} - P_{P,COG}}{P_{P,SEP}} \cdot 100$$

III. Results

A. Loads and generation

In Fig.4, firstly, the electrical demand from buildings 3 and 4 of ENEA is illustrated, followed by the electrical powers of the installations. These results were obtained by prioritizing, to meet the electrical load, as follows: PV system Nr.1, PV system Nr.2, electrical storage system, wind turbine, and finally, the cogenerator. As a working hypothesis, it is assumed that the cogenerator tracks the electrical load and does not drop below 25 kW_{el}. The electrical load, in blue, represents the sum of the power demand from utilities, such as lights, computers, winter and summer room conditioning through heat pumps and refrigeration machines, respectively. It also considers units 4 and 6 of the CRESCO Laboratory. It is observed that the electrical load of buildings 3 and 4, moment by moment, is always high and never drops to zero. This is attributed to the presence of the supercomputer, which requires high electrical power. It has been estimated that more than 80% of the electrical demand of building 3and 4 is attributed to CRESCO, both for server power and cooling.
In yellow, the total producibility of PV systems Nr.1 and Nr.2 is shown. As can be observed, there is a peak of 174 kW between June 27th and 28th around 12:20 pm. However, it is interesting to observe that the difference between summer and spring days is not significant because, on hot days, the panel reaches high temperatures, reducing its efficiency. It

has been observed that powers exceeding 170 kW are almost always reached in June.

In green, the electrical producibility of the wind turbine system, consisting of four 1.5 kW wind turbines each, is shown. These turbines start producing when the wind speed in Portici exceeds 2 m/s and turn off for speeds exceeding 15 m/s. From the graph, it can be observed that one often operates at the nominal point of 6 kW total power, as this power is reached for wind speeds of 12 m/s, which are easily achievable. Compared to PVs, it is able to produce even at night. Finally, in red, the electrical production of the cogenerator is shown. With the working hypothesis made, i.e., that the CHP tracks the electrical load, it can be seen that the cogenerator remains always on and operates almost always at the nominal point of 50 kWel and very rarely at partial load. It is worth noting that the engine remains always on because it was the first choice in the first control strategies of the SEM.

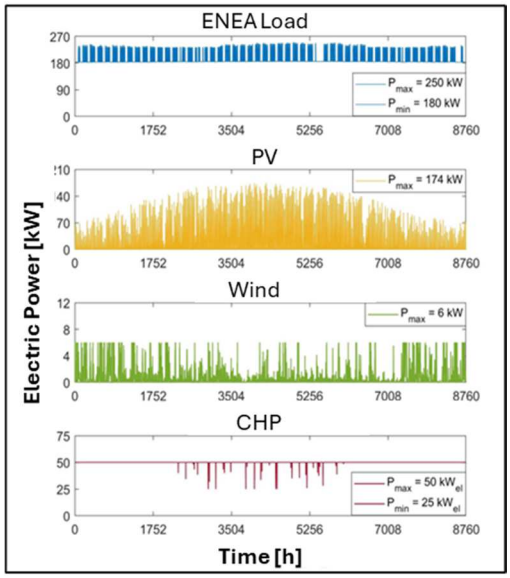

Fig.4 Load and Electric power provided by PV, Wind and CHP

B. *Control Strategy 1*

In the first strategy, it was assumed that the Combined Heat and Power (CHP) system was electrically driven. In Fig. 5 starting from the graph in blue, which depicts power, it is evident that the PV system alone is never able to fully meet the user's demand if operated independently, as it would always require power from the grid. This reasoning also applies when adding only wind power (in yellow) to the PV system. However, when considering the combined output of PV, wind, and CHP, as dictated by the first control strategy, there are hours throughout the year where is capable to supply power to the grid, with a peak of 9 kW. Analyzing the power required from the grid separately, it is deduced that the CHP alone can sell power to the grid. Translating this into electrical energy, in

Fig. 6, it can be observed that when supplying power solely from the PV system, the purchase of electrical energy linearly increases over time, totaling 1509 MWh, derived from the difference between the electrical energy required by ENEA in a year and the useful electrical energy provided by the PV systems. Consequently, the electrical energy sold to the grid by the PV systems is 0 MWh, as seen in the rightmost graph in Fig. 6. The same conclusion is reached when operating solely with PV and wind power, totaling 1502 MWh, reduced by the portion of useful electrical energy that the wind power system can provide. The discussion remains identical in terms of electrical energy sold to the grid, also amounting to 0 MWh. Slightly different is the scenario when operating with all three systems, as there are hours where the CHP's power output exceeds its electrical demand. Therefore, the trend of electrical energy purchased from the grid is not linear. With the presence of the cogenerator, the final electrical energy purchased from the grid amounts to 1065 MWh. In the graph on the far right, it is observed that when aiming to satisfy the entire electrical load with all systems, there is a small portion of electrical energy that we sell to the grid, totaling 37 kWh.

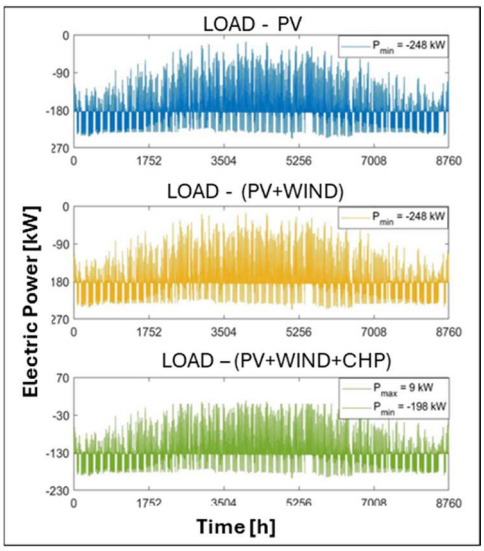

Fig. 5 Load and generation 1st strategy

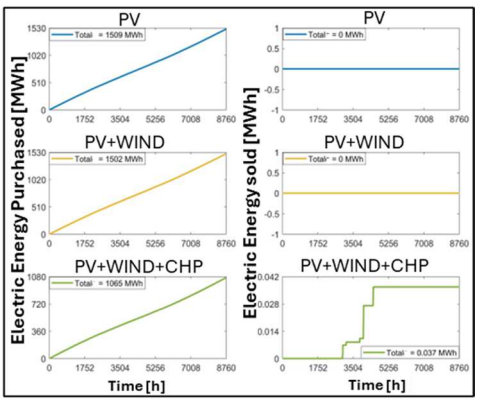

Fig. 6 Results of the 1st strategy

C. *Control Strategy 2*

From the analysis of the results of the first control strategy, the idea arose to evaluate the local Primary Energy Saving (PES) of the CHP subsystem. The second control strategy involves shutting down the engine whenever the PES of the cogeneration subsystem is negative. This second analysis was conducted using Matlab environment [21]. From the analysis of Fig. 7, which relates to the PES of the cogeneration subsystem, it is observed that for all hours of the year, the PES is consistently negative. In practical terms, this means that activating the CHP does not lead to savings in fossil primary energy.

It has been mentioned that for the second control strategy, a PES less than zero corresponds to shutting down the CHP. Indeed, from the yellow graph, it can be observed that the engine never delivers electrical power. Similarly, it never generates waste heat, so in the winter months, the heat demand for space heating is provided by the heat pump. Additionally, it is noted that the purchased electrical energy equals the electrical energy purchased as seen in the first strategy if the electrical demand is solely supplied by PV and wind power. Hence, the 437 MWh from the CHP are no longer available, leading to the purchase of 1502 MWh of Finally, it can be observed that the electricity fed into the grid is zero because, as seen in the first control strategy, the only component of the micro-grid that supplied electricity to the grid was the CHP, which is now shut down in the second strategy.

Fig. 7 Results of the 2nd strategy

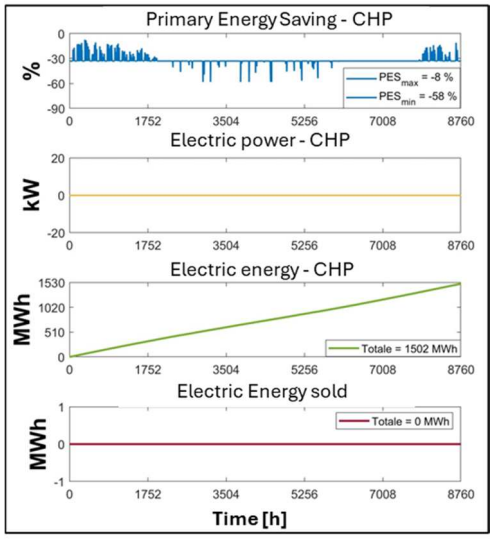

D. Control Strategy 3

In this control strategy, it was hypothesized that the waste heat from the cogenerator, in addition to meeting the thermal demand for space heating, also satisfies the production of domestic hot water, which is not considered in the actual micro-grid. In the real micro-grid, the production of domestic hot water is achieved through diesel-fed boilers. The model configuration remains unchanged, but with the addition of the boiler. From the analysis of Figure 8, it can be observed that the Primary Energy Saving (PES) is greater than zero for only a few hours of the year, approximately 682 hours, distributed throughout the year. The highest PES values are obtained when there is also a demand for thermal power for heating, so in the first months of the year and the last months of the year. PES values greater than zero are also found when heating is not required, but at the maximum power required for domestic hot water (DHW) production, which is 46.35 kW. In accordance with the third strategy, the engine is on for only about 682 hours for a useful electrical energy production of 34 MWh, equal to the energy produced. Therefore, from the last graph, it can be seen how the total electrical energy purchased from the grid decreases from 1502 MWh to 1468 MWh, and the total electrical energy sold to the grid is zero. strategy, with the CHP running for all hours of the year: 14.53 MWh versus 6.32 MWh.

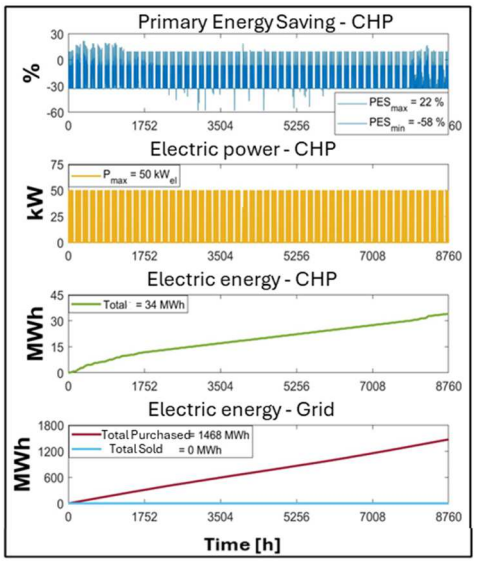

Figure 8 Results of the 3rd strategy

E. Discussion

From the comparison in Table II, it can be immediately observed that the primary energy savings of the second control strategy, with the CHP turned off for all hours of the year, are more than double compared to the first control The first difference lies in the separate primary energy, where in the second control strategy, we do not have electrical surplus, resulting in a slightly lower separate primary energy compared to the first strategy. The significant difference is therefore made by the primary energy of the SEM system, cogenerated: 3264 MWh for the SEM compared to 3578 MWh for the 1st strategy. In terms of absolute savings, it is observed that in the second strategy, the savings are more than two times that of the first strategy. The same can be stated for CO_2 emissions (TABLE III), with avoided emissions savings for the second strategy nearly three times the avoided emissions savings of the first strategy: 14.53 tons versus 4.77 tons.

TABLE II Comparison of Strategies on Primary Energy supply

Model – Load – Chp – Boiler	**$E_{P,SEP}$ [MWh/year]**	**$E_{P,COG}$ [MWh/year]**	**Δ_{EP} [MWh/year]**	**TPES* [%]**
SEM – ENEA – On – No	3819.70	3578.31	241.39	**6.32**
SEM – ENEA – Off – No	3819.61	3264.61	555.00	**14.53**
SEM – ENEA – On/Off – Yes	3919.77	3357.80	561.97	**14.33**

b. * Total Primary Energy Saving

TABLE III Comparison of Strategies on CO_2 emission

Model – Load – CHP – Boiler	**mCO_2, SEP [ton/year]**	**mCO_2, COG [ton/year]**	**ΔmCO_2 [ton/year]**	**ΔmCO_2 [%]**
Sem – Enea – On – No	448.05	426.65	21.40	4.77
Sem – Enea – Off – No	448.04	382.94	65.10	14.53
Sem – Enea – On/Off – Yes	474.78	404.70	70.08	14.76

It can be observed that the addition of the boiler in the third strategy yields nearly the same results as the second control strategy compared to the first, with a percentage primary

energy savings of more than double and nearly triple the avoided emissions savings. However, when comparing the second and third strategies, it is noted that in the configuration without the boiler and with the CHP always off, there are slight advantages, in percentage terms, compared to the configuration with the boiler and the engine either on or off depending on the PES of the CHP. This can be attributed to the fact that in the third strategy, the engine is only on for 682 hours in a year, consequently, the integration of heat from the boiler into the cogenerative system is significant, amounting to approximately 62 MWh of thermal energy out of the 89 MWh required to produce hot water for sanitation for a duration of 2408 h/year. This means that approximately 70% is satisfied by the boiler and not by the waste heat from the thermal engine.

IV. Conclusion

In this study, a model of polygeneration hybrid system design to be installed at the ENEA research center in Portici was developed using TRNSYS environment. This model allowed for the simulation of ENEA's micro-grid and a detailed energy analysis regarding primary energy savings and avoided CO_2 emissions compared to the traditional system. This analysis was extended to multiple control strategies, including three strategies considered alongside a proposed alternative design. In each strategy, priority was given to renewables, followed by the cogenerator and then the grid to meet electrical demand. Thermal load was met by the recoverable thermal power from the engine. Results underscored the importance of control strategies, as the second strategy yielded over double and nearly triple the primary energy savings and CO_2 emissions avoidance compared to the first one, respectively, with the third control strategy showing similar albeit slightly lower savings. Future improvements for this work could involve accurately understanding the electrical and thermal characteristics of the actual components constituting the micro-grid. Additionally, improving the precision of the storage system modeling by considering $LiFePO_4$ batteries, rather than lead-acid batteries, could enhance the study's accuracy.

Acknowledgment

This research was funded by the Ministry of Ecological Transition under the Contract Agreement "Accordo di Programma Mission Innovation 2021 – 2024 – project MISSION Multivector Integrated Smart Systems and Intelligent microgrids for accelerating the energy transitiON".

References

[1] S. Fabozzi, G. Graditi, and M. Valenti, "Techno-economic design of a smart multienergy microgrid," 2022 AEIT International Annual Conference, AEIT 2022, 2022, doi: 10.23919/AEIT56783.2022.9951736.

[2] M. A. Hoummadi et al., "A review of constraints and adjustable parameters in microgrids for cost and carbon dioxide emission reduction," Heliyon, p. e27489, Mar. 2024, doi: 10.1016/J.HELIYON.2024.E27489.

[3] G. Adinolfi, R. Ciavarella, G. Graditi, A. Ricca, and M. Valenti, "A Planning Tool for Reliability Assessment of Overhead Distribution Lines in Hybrid AC/DC Grids," Sustainability 2021, Vol. 13, Page 6099, vol. 13, no. 11, p. 6099, May 2021, doi: 10.3390/SU13116099.

[4] A. Bonfiglio, F. Delfino, F. Pampararo, R. Procopio, M. Rossi, and L. Barillari, "The Smart Polygeneration Microgrid test-bed facility of Genoa University," Proceedings of the Universities Power Engineering Conference, 2012, doi: 10.1109/UPEC.2012.6398656.

[5] M. Di Somma et al., "Stochastic Operation Optimization of the Smart Savona Campus as an Integrated Local Energy Community Considering Energy Costs and Carbon Emissions," Energies 2022, Vol. 15, Page 8418, vol. 15, no. 22, p. 8418, Nov. 2022, doi: 10.3390/EN15228418.

[6] M. Panwar et al., "Dispatch in Microgrids: Lessons from the Fort Collins Renewable and Distributed Systems Integration Demonstration Project," The Electricity Journal, vol. 25, no. 8, pp. 71–83, Oct. 2012, doi: 10.1016/J.TEJ.2012.09.011.

[7] A. Buonanno, M. Caliano, M. Di Somma, G. Graditi, and M. Valenti, "Comprehensive method for modeling uncertainties of solar irradiance for PV power generation in smart grids," SEST 2021 - 4th International Conference on Smart Energy Systems and Technologies, Sep. 2021, doi: 10.1109/SEST50973.2021.9543245.

[8] S. Fabozzi, G. Graditi, and M. Valenti, "ENEA SEM: Design of a Test-Bed for Research, Testing and Development in Smart Multienergy System Sector," 2022 Workshop on Blockchain for Renewables Integration, BLORIN 2022, pp. 182–187, 2022, doi: 10.1109/BLORIN54731.2022.10028045.

[9] B. Simone, G. Alfredo, I. Raffaele, K. Alì, M. Massimiliano, and P. H. Trieu, "Battery–integrated combined cooling, heating and power plant (CCHP) through NH3 – H2O absorption system in a hospital facility," J Phys Conf Ser, vol. 2648, no. 1, p. 012020, Dec. 2023, doi: 10.1088/1742-6596/2648/1/012020.

[10] M. Pipicelli, M. Muccillo, and A. Gimelli, "Influence of the control strategy on the performance of hybrid polygeneration energy system using a prescient model predictive control," Appl Energy, vol. 329, p. 120302, 2023, doi: 10.1016/j.apenergy.2022.120302.

[11] A. Gimelli et al., "Optimal configuration of modular cogeneration plants integrated by a battery energy storage system providing peak shaving service," Appl Energy, vol. 242, pp. 974–993, May 2019, doi: 10.1016/J.APENERGY.2019.03.084.

[12] K. S. A., "TRNSYS-A transient system simulation program.," University of Wisconsin-Madison, Engineering Experiment Station Report, pp. 38–12, 1988, Accessed: Mar. 12, 2024. [Online]. Available: https://cir.nii.ac.jp/crid/1571135649123141888

[13] A. Carotenuto et al., "Energy analysis of a small geothermal district heating system in Southern Italy," International Journal of Heat and Technology, vol. 34, no. Special Issue 2, pp. S519–S527, 2016, doi: 10.18280/IJHT.34S246.

[14] F. Calise, S. Fabozzi, L. Vanoli, and M. Vicidomini, "A sustainable mobility strategy based on electric vehicles and photovoltaic panels for shopping centers," Sustain Cities Soc, vol. 70, p. 102891, Jul. 2021, doi: 10.1016/J.SCS.2021.102891.

[15] "TRNSYS 17 Volume 4 Mathematical Reference PDF | PDF | Control Theory | Hvac." Accessed: Mar. 13, 2024. [Online]. Available: https://it.scribd.com/document/313103671/TRNSYS-17-Volume-4-Mathematical-Reference-pdf

[16] "TRNSYS 18," 2017, Accessed: Mar. 13, 2024. [Online]. Available: http://sel.me.wisc.edu/trnsyshttp://software.cstb.frhttp://www.tess-inc.com

[17] "Mission Innovation | Mission Innovation site." Accessed: Mar. 19, 2024. [Online]. Available: https://mission-innovation.it/

[18] J. H. Eckstein, "Detailed modelling of photovoltaic system components," 1990, Accessed: Mar. 13, 2024. [Online]. Available: https://minds.wisconsin.edu/bitstream/handle/1793/45596/Eckstein1990.pdf

[19] T. U. Townsend, "A Method for Estimating the Long-Term Performance of Direct-Coupled Photovoltaic Systems," 1989, Accessed: Mar. 13, 2024. [Online]. Available: https://minds.wisconsin.edu/handle/1793/46720

[20] "Cogeneratore: Vitobloc 200 EM 50/81 | Viessmann IT." Accessed: Mar. 12, 2024. [Online]. Available: https://www.viessmann.it/it/prodotti/cogeneratore/vitobloc-200-em-50-81.html

[21] "MathWorks - Makers of MATLAB and Simulink - MATLAB & Simulink." Accessed: Mar. 13, 2024. [Online]. Available: https://www.mathworks.com./